Limnol. Oceanogr., 34(8), 1989, 1545–1562

Surface pigments, algal biomass profiles, and potential production of the euphotic layer: Relationships reinvestigated in view of remote-sensing applications

André Morel and Jean-François Berthon
Laboratoire de Physique et Chimie Marines, Université Pierre et Marie Curie, BP 8, F 06230 Villefranche-sur-Mer, France

Abstract

Maps of surface chlorophyllous pigment (Chl *a* + Pheo *a*) are currently produced from ocean color sensors. Transforming such maps into maps of primary production can be reliably done only by using light-production models in conjunction with additional information about the column-integrated pigment content and its vertical distribution.

As a preliminary effort in this direction, ~4,000 vertical profiles of pigment (Chl *a* + Pheo *a*) determined only in oceanic Case 1 waters have been statistically analyzed. They were scaled according to dimensionless depths (actual depth divided by the depth of the euphotic layer, Z_e) and expressed as dimensionless concentrations (actual concentration divided by the mean concentration within the euphotic layer). The depth Z_e, generally unknown, was computed with a previously developed bio-optical model. Highly significant relationships were found allowing $\langle C \rangle_{tot}$, the pigment content of the euphotic layer, to be inferred from the surface concentration, C_{pd}, observed within the layer of one penetration depth. According to their $\bar{C}_{pd}$ values (ranging from 0.01 to >10 mg m^{-3}), we categorized the profiles into seven trophic situations and computed a mean vertical profile for each. Between a quasi-uniform profile in eutrophic waters and a profile with a strong deep maximum in oligotrophic waters, the shape evolves rather regularly. The well-mixed cold waters, essentially in the Antarctic zone, have been separately examined. On average, their profiles are featureless, without deep maxima, whatever their trophic state. Averaged values of ρ, the ratio of Chl *a* to (Chl *a* + Pheo *a*), have also been obtained for each trophic category.

The energy stored by photosynthesizing algae, once normalized with respect to the integrated chlorophyll biomass $\langle C \rangle_{tot}$ is proportional to the available photosynthetic energy at the surface via a parameter ψ^*, which is the cross-section for photosynthesis per unit of areal chlorophyll. By taking advantage of the relative stability of ψ^*, we can compute primary production from ocean color data acquired from space. For such a computation, inputs are the irradiance field at the ocean surface, the "surface" pigment from which $\langle C \rangle_{tot}$ can be derived, the mean ρ value pertinent to the trophic situation as depicted by the $\bar{C}_{pd}$ or $\langle C \rangle_{tot}$ values, and the cross-section ψ^*. Instead of a constant ψ^* value, the mean profiles can be used; they allow the climatological field of the ψ^* parameter to be adjusted through the parallel use of a spectral light-production model.

Acknowledgments

The support of the Centre National de la Recherche Scientifique (under contract CNRS/UA 353) and of the Centre National d'Etudes Spatiales (under contract 88/1285) are duly acknowledged. We express particular appreciation to A. Bricaud and to the unknown referees for their constructive criticisms.

Beside the "BNDO" data, obtained thanks to B. Voituriez and N. Cloatre, many detailed data have been obtained as personal communications or as unpublished reports. In reference to the numbers in Table 1, we acknowledge the help of M. Innamorati and L. Lazzara (4, 5, 27), J. H. Hecq and A. Goffart (6, 26), P. Raimbault and C. Millot (7), J. Neveux (9), R. T. Barber (10, 11), P. Brown (12), P. Raimbaud, H. J. Minas, and B. Coste (13), G. Anderson and F. Thomas (15), S. El Sayed (18, 19, 23), W. Gieskes (25), and G. Jacques, M. Panouse, and M. Eckernkemper (28).

This work is a contribution to the research encouraged by the IAPSO Commission "Oceanography from Space."

Determination of the time-varying flux of carbon (and associated elements) in the world ocean is a focused objective of programs such as JGOFS (1988) and IGBP (1988). Photosynthetic carbon fixation by phytoplanktonic algae in the euphotic zone of the ocean remains controversial, but is thought to be comparable in magnitude to that effected by the terrestrial phytosphere (Martin et al. 1987; Berger et al. 1987). The temporal and spatial requirements of global monitoring of marine photosynthesis can be met only by satellites, under the proviso that "chlorophyll maps" produced from the data delivered by ocean color sensors can be transformed into "production maps."

With the improved capabilities of future ocean color sensors (e.g. SeaWIFS 1987) and

with a parallel refinement of algorithms, we can reasonably anticipate that accurate determination of the chlorophyllous pigment concentrations within the upper layer will be within reach. We also optimistically assume that the various physiological processes which control the light-harvesting and photosynthesis capabilities of algae will be adequately parameterized. Meaningful use of the light-photosynthesis models that already exist (Platt et al. 1988; Sathyendranath et al. 1989; Morel 1989) requires improved knowledge of the physiological parameters, inasmuch as the physical and climatological aspects of primary production can be safely and accurately modeled at present.

Even in such an optimistic perspective, a major problem remains. On one hand, production models which apply to the entire euphotic layer use the vertical profile of pigment biomass as input. On the other hand, and due to unavoidable (physical) limitations, only the pigment content within the upper attenuation length (the "penetration depth" according to Gordon and McCluney 1975) is accessible to remote-sensing techniques. Therefore, a gap exists between this partial information and what is needed when operating a model. In this paper we attempt to fill this gap by examining whether it is possible to derive statistically significant relationships between the pigment concentration in the upper layer, the pigment content within the productive column, and, tentatively, the shape of the vertical biomass profile.

The underlying guideline when searching for the existence of such relationships rests on two common observations.

- In stratified oligotrophic oceanic areas, where nutrient depletion occurs in the upper layers, a deep chlorophyll maximum often develops (e.g. *see* Jamart et al. 1977; Herbland and Voituriez 1979; Dandonneau 1979; Cullen 1982).
- When vertical mixing or active upward transport bring nutrients into the well-lit surface layer, eutrophic situations are quickly created leading to high biomass concentrated within a thin euphotic layer; this layer is relatively well mixed and likely homogeneous with respect to its biomass profile; such conditions are encountered in coastal upwelling areas or during the vernal bloom at moderate and high latitudes.

It can be intuitively presumed that a regular trend takes place between these extreme and typical situations. For instance, mesotrophic waters of the equatorial upwelling belt also exhibit a deep chlorophyll maximum, yet one less pronounced and generally shallower than that occurring in oligotrophic zones. Nevertheless, exceptions to this heuristic scheme are a priori to be expected. The deep convection which occurs during winter at high and to a lesser extent at moderate latitudes (Levitus 1982; Glover and Brewer 1988) results in penetrative mixed layers where the remnant biomass is very likely homogeneously distributed. Even in summer, most of the southernmost Antarctic, weakly stabilized, waters remain oligotrophic, without exhibiting a distinct deep chlorophyll maximum. Separate examination of these "exceptional" situations must be envisaged.

With the same motivation in mind, Platt and Sathyendranath (1988) recently proposed a "generalized biomass profile" to be used in models with a view of predicting carbon fixation, first at regional and then at global scales. Also they pointed out that useful field activity in the future would "establish the typical shape of the biomass profile," with the underlying assumption that "for a given region of the ocean, in a given season, this shape is stable." In the present study historical data are reviewed and a statistical analysis is carried out by considering about 4,000 stations (pigment profiles), widely distributed in the world ocean. This analysis is not made on a geographical basis (except for separate examination of the deep mixed-layers situations). Instead, the criterion adopted is the trophic state (the integrated biomass)—regardless of region or season. These profiles have been preliminarily examined and selected (from among ~6,000 stations) as representative of Case 1 waters only. Under this condition the depth of the euphotic layer can be computed (Morel 1988) and from there the profiles can be properly scaled for comparison by using a dimensionless depth, defined as the ratio

of the actual depth to that of the euphotic layer.

Data

The biological database used here is summarized in Table 1. The data were extracted from the "Banque Nationale des Données Océanographiques" in Brest (BNDO) and from oceanographic cruise reports or papers found in the literature. Among the 4,742 stations archived in BNDO, only 2,811 were used in this study; 1,347 were rejected because they were identified as being, or suspected to be, "turbid Case 2" waters (Morel and Prieur 1977); 584 others were disregarded because of an incomplete set of data with respect to depth. The same sorting was effected for the data found in other sources. The geographic distribution of the different stations (Fig. 1) reveals as usual an uneven coverage: the East Atlantic and Southwest Pacific are well documented, whereas other Pacific zones are poorly represented. Winter stations at high latitudes are infrequent (apart from 14 stations in the North Pacific at, or in the vicinity of, Ocean Weather Station P). Austral summer stations in Antarctic areas are rather numerous.

The range of integrated pigment content, $\langle C \rangle_{tot}$, within the euphotic layer is wide, from ~ 2 mg m^{-2} to >300 and encompasses all trophic situations occurring in the open ocean. The number of stations representing very oligotrophic or very eutrophic situations, with $\langle C \rangle_{tot} \leq 10$ mg m^{-2} or ≥ 90, remains relatively low compared to that of intermediate situations.

For about half of the stations Chl *a* and Pheo *a* concentrations were separately determined; for the rest, only one "pigment concentration" was available (meaning that Chl *a* and Pheo *a* are pooled together). (*See list of symbols for definitions and units.*) For $<7\%$ of the stations, optical data exist and the depth of the euphotic layer is known, but for most of the profiles, the unknown euphotic depth must be computed.

Methods

Computation of the euphotic depth Z_e— This depth is defined as that where the downwelling PAR irradiance is reduced to 1% of its value at the surface. When not measured, Z_e is derived from the pigment concentration profile itself, thanks to a relationship which links Z_e to the total pigment content $\langle C \rangle_{tot}$ within the euphotic layer (0 to Z_e). A spectral model of downwelling radiation penetration as a function of the phytoplankton pigment concentration has been developed (Morel 1988). After integrating over the appropriate (photosynthetic) spectral range (400–700 nm), the ratio of PAR at any depth to PAR just below the surface can be computed; in particular the depth where this ratio is 1% can be determined as well as the total pigment content within the above-lying column (Morel 1988, equation 11 and figure 2). This relationship between Z_e and $\langle C \rangle_{tot}$ is shown as a solid curve in Fig. 2. The curvature accounts for the fact that Z_e tends toward a limiting value (about 183 m) for pure water, i.e. when $\langle C \rangle_{tot}$ tends toward zero.

For computational convenience, this curve is approximated by two successive expressions,

$$Z_e = 568.2 \langle C \rangle_{tot}^{-0.746} \quad \text{when } Z_e < 102 \text{ m} \qquad (1a)$$

and

$$Z_e = 200.0 \langle C \rangle_{tot}^{-0.293} \quad \text{when } Z_e > 102 \text{ m}, \qquad (1b)$$

shown as dashed lines in the log-log representation of Fig. 2. Note that the first equation also results from a direct linear regression analysis performed on the log-transformed data concerning Z_e and the mean pigment concentration within the euphotic layer (equation 3 of Morel 1988).

The simultaneous computations of Z_e and $\langle C \rangle_{tot}$ from the actual pigment profile used in conjunction with Eq. 1a and (or) 1b are as follows. A given pigment profile is progressively integrated with respect to increasing depth (z). The successive integrated pigment values are introduced in Eq. 1a, thus providing successive "Z_e" values that are progressively decreasing. Once the last Z_e value, as obtained, becomes lower than the z depth used when integrating the profile, the process is stopped and reversed. Then an iterative scheme allows the exact Z_e depth to be determined by interpolating (increment 0.1 m); $\langle C \rangle_{tot}$ is produced at the same

Table 1. Relevant information concerning the cruises used in the present study.

	Cruise	*N*	Location	Reference	No.
1969/1986	BNDO data bank	2,811	World ocean		(1)
1964	*Calypso*	5	Tyrrhenian Sea	*Calypso* 1969	(2)
1969	MEDIPROD 1	96	Western Mediterranean	Mediprod 1 1971	(3)
1983	Elba 2	26	Tyrrhenian Sea	Innamorati et al. 1989*a*	(4)
1985	Alto Tirreno 1	38	Tyrrhenian Sea	Unpubl.	(5)
1984		25	Western Mediterranean	Hecq et al. 1986	(6)
1986	MEDIPROD 5	87	Western Mediterranean	Unpubl.	(7)
1970	SCOR WG15/*Discoverer*	18	Sargasso Sea, Gulf of Mexico, tropical East Pacific	SCOR—Working Group 15 1973	(8)
1987	CHLOMAX	26	Sargasso Sea	Unpubl.	(9)
1975	CUEA Joint 1	22	Mauritanian upwelling	CUEA-Joint 1 1975	(10)
1977	CUEA Joint 2	110	Peruvian upwelling	CUEA-Joint 2 1975	(11)
1985		46	South Benguela upwelling	Brown and Henry 1985	(12)
1986	PACIPROD	46	Peruvian upwelling and Galapagos zone	Paciprod 1989	(13)
1982	California	10	Northern Gulf of California	Alvarez-Borrego and Gaxiola-Castro 1988	(14)
1969	Station P	83	Gulf of Alaska	Anderson et al. 1977	(15)
1979	Vector/*Endeavour*	18	Vancouver Island, Juan de Fuca Strait	Unpubl.	(16)
1985	*Melville*	3	North Pacific	Laws et al. 1987	(17)
1970	*Eltanin* 46	9	South Pacific Antarctic	Unpubl.	(18)
1972	*Eltanin* 51	18	South Atlantic Antarctic	Unpubl.	(19)
1977	ANTIPROD 1	26	South Indian Antarctic	Antiprod 1 1978	(20)
1980	ANTIPROD 2	17	South Indian Antarctic	Antiprod 2 1982	(21)
1984	APSARA 2—ANTIPROD 3	32	South Indian Antarctic	Apsara 2—Antiprod 3 1987	(22)
1984	*Polarstern*	38	Bransfield Strait/Elephant Island	Unpubl.	(23)
1985	INDIGO 1	22	South Indian	Indigo 1 1988	(24)
1986		41	Weddell Sea	Elbrächter et al. 1987	(25)
1987	INDIGO 3	20	South Indian Antarctic	Goffart and Hecq 1988	(26)
1988	ANTARTIDE	36	Terra Nova Bay Antarctic	Innamorati et al. 1989*b*	(27)
1988/1989	ANTARKTIS 7/EPOS 2	77	South Atlantic Antarctic	Unpubl.	(28)
		3,806			

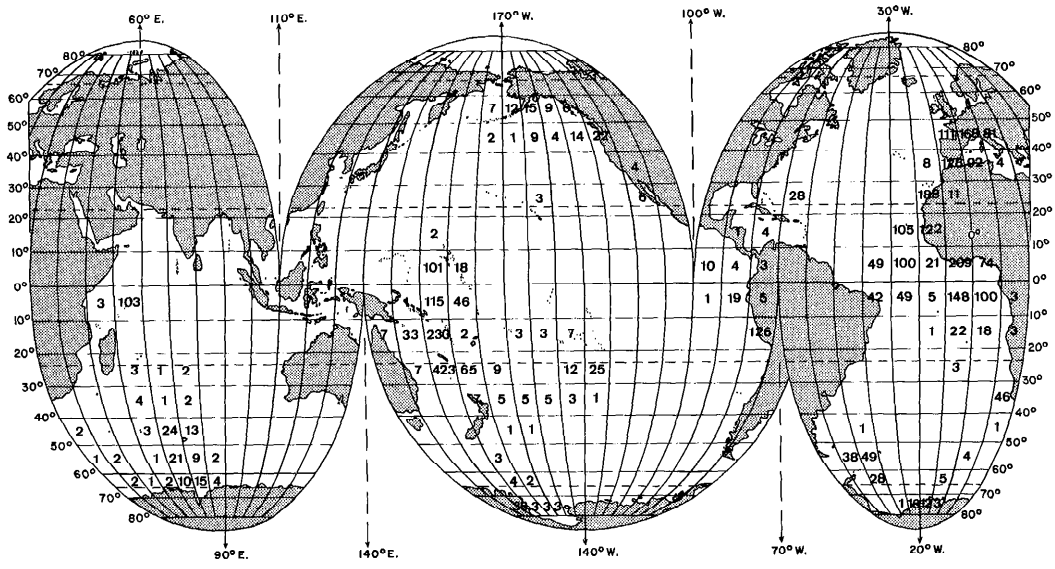

Fig. 1. Geographic distribution of the stations (3,806) used in the present study.

time. There is no particular problem in switching from Eq. 1a to 1b if Z_e exceeds 102 m.

Mean pigment concentration within the euphotic layer and within the surface layer— The determination (or the measurement) of Z_e allows $\bar{C}_{Ze}$, the mean pigment concentration within the euphotic layer, to be computed as

$$\bar{C}_{Ze} = Z_e^{-1} \int_0^{Z_e} C(z)\, dz$$
$$= Z_e^{-1} \langle C \rangle_{\text{tot}}.$$

The "surface" layer is defined as having a thickness corresponding to one attenuation length with respect to PAR; the corresponding depth, Z_{pd}, also called the penetration depth (Gordon and McCluney 1975), is therefore

$$Z_{pd} \simeq Z_e/4.6$$

and the mean pigment concentration within this layer is

$$\bar{C}_{pd} = Z_{pd}^{-1} \int_0^{Z_{pd}} C(z)\, dz.$$

A common use is to define a "weighted" mean concentration within the surface layer, which accounts for the fact that the optical contribution to reflectance from a layer dz, located at a depth z, is damped by a factor $\exp(-2kz)$, where k is a mean attenuation coefficient valid for the downwelling and upwelling irradiances. This averaged concentration, $\bar{C}_{\text{sat}}$, presumably "seen" by a remote sensor, is computed as follows:

$$\bar{C}_{\text{sat}} = \frac{\int_0^{Z_{pd}} C(z)\exp(-2kz)\, dz}{\int_0^{Z_{pd}} \exp(-2kz)\, dz}$$

where k is here taken as being the attenuation coefficient for the downwelling PAR irradiance and, by approximation, is equal to $4.6/Z_e$.

Mean pigment profiles—As information about the vertical structure of the pigment distribution is definitely not accessible by remote sensing, we attempted to determine typical "mean profiles" for various trophic situations characterized by their pigment concentration in the upper layer, $\bar{C}_{pd}$ (or by their column-integrated pigment content $\langle C \rangle_{\text{tot}}$, if a reliable relationship between $\bar{C}_{pd}$ and $\langle C \rangle_{\text{tot}}$ is proven to exist). All the profiles were accordingly sorted into seven categories for the open ocean (high latitude waters excepted) and into two categories for Antarctic and North Pacific waters (in win-

Significant symbols

Chl *a*, Pheo *a*	Chl *a* and pheophytin *a* concentration, mg m^{-3}
ρ	Chl *a*/(Chl *a* + Pheo *a*) ratio
C	Total pigment (Chl *a* + Pheo *a*) concentration, mg m^{-3}
Z	Depth, m
Z_e	Euphotic depth, m
ζ	Normalized depth with respect to Z_e, $\zeta = Z/Z_e$
$\bar{C}_{Ze}$	Mean pigment concentration within the euphotic layer, mg m^{-3}
$\langle C\rangle_{tot}$, $\langle Chl\rangle_{tot}$	Total pigment and total Chl *a* content within the euphotic layer, mg m^{-2}
$\langle C\rangle_z$	Total pigment content within a layer of thickness z, mg m^{-2}
Z_{pd}	Penetration depth (=$1/k$), m
k	Attenuation coefficient for downwelling PAR irradiance, m^{-1}
$\bar{C}_{pd}$	Mean pigment concentration within the surface layer (one penetration depth), mg m^{-3}
$\bar{C}_{sat}$	Weighted mean pigment concentration within the surface layer, mg m^{-3}
PAR	Photosynthetically available radiation, W m^{-2}
$\overline{PAR}(0^+)$	PAR just above the surface and integrated over the daylength, J m^{-2}
$\overline{PSR}$	Daily photosynthetically stored radiant energy within the euphotic layer, J m^{-2}
ψ^*	Cross-section for photosynthesis per unit of areal chlorophyll, m^2 (g Chl)$^{-1}$
P	Daily carbon fixation by algae within the productive layer, g C m^{-2} d^{-1}
$P(z)$	Primary production at depth z, g C m^{-3} d^{-1}
$\bar{P}(0, Z_e)$	Mean primary production within the euphotic layer $= Z_e^{-1} \int_0^{Z_e} P(z)\,dz$, g C m^{-3} d^{-1}

ter). For each category (*see Table 3*), the following normalizations were effected: to compare the profiles on the basis of a "dimensionless" depth, ζ, the actual z values were divided by Z_e computed (or observed) at the station in question; each $C(z)$ value was normalized with respect to the mean pigment concentration within the euphotic layer, $\bar{C}_{Ze}$, and thus the shape of the vertical profiles (for different stations) can be compared regardless of their absolute magnitude. Both these normalizations provide nondimensionalized profiles which, whatever their pigment contents, can be superimposed or pooled together to compute a mean profile for each category. For each station, the water column was divided into

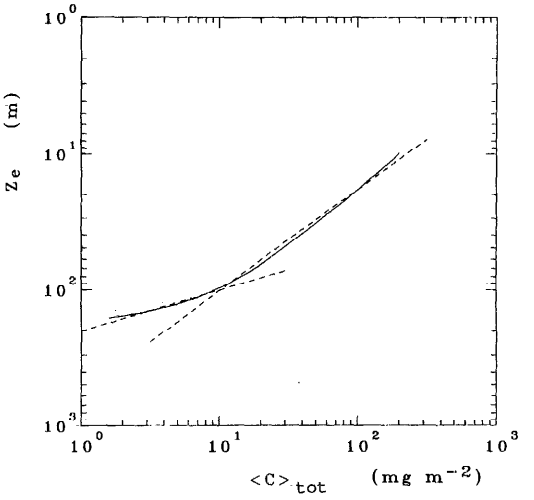

Fig. 2. Depth of the euphotic layer Z_e vs. the total pigment content within the euphotic layer $\langle C\rangle_{tot}$. The solid curve represents the relationship obtained with a spectral model of photosynthetic downward radiation propagation (Morel 1988). The dashed lines represent Eq. 1a ($\langle C\rangle_{tot} > 10$ mg m^{-2}) and b ($\langle C\rangle_{tot} \le 10$ mg m^{-2}) used when computing Z_e (*see text*).

Table 2. Statistical relationships between total pigment content in the water column $\langle C\rangle_{tot}$ (mg m^{-2}) and mean pigment concentrations within the surface layer, expressed as $\bar{C}_{pd}$ or $\bar{C}_{sat}$ (mg m^{-3}); the r^2 values are for the log-transformed data.

Stratified waters (low and moderate latitudes, 3,497 stations)		
$\langle C\rangle_{tot} = 40.6\ \bar{C}_{pd}^{0.460}$	$r^2 = 0.872$	(2a)
$\langle C\rangle_{tot} = 40.6\ \bar{C}_{sat}^{0.459}$	$r^2 = 0.869$	(3a)
For $\bar{C}_{pd}$ or $\bar{C}_{sat} \le 1.0$ mg m^{-3}		
$\langle C\rangle_{tot} = 38.0\ \bar{C}_{pd}^{0.425}$	$r^2 = 0.686$, $n = 2{,}904$	(2b)
$\langle C\rangle_{tot} = 38.0\ \bar{C}_{sat}^{0.423}$	$r^2 = 0.681$, $n = 2{,}905$	(3b)
For $\bar{C}_{pd}$ or $\bar{C}_{sat} > 1.0$ mg m^{-3}		
$\langle C\rangle_{tot} = 40.2\ \bar{C}_{pd}^{0.507}$	$r^2 = 0.776$, $n = 593$	(2c)
$\langle C\rangle_{tot} = 40.3\ \bar{C}_{sat}^{0.505}$	$r^2 = 0.767$, $n = 592$	(3c)
Well-mixed waters (high latitudes, 309 stations)		
$\langle C\rangle_{tot} = 38.0\ \bar{C}_{pd}^{0.551}$	$r^2 = 0.933$	(4)
$\langle C\rangle_{tot} = 37.9\ \bar{C}_{sat}^{0.548}$	$r^2 = 0.930$	(5)

The straight lines (in log-log representation) which correspond to Eq. 2b and c on one hand and 3b and c on the other intersect at $\bar{C}_{pd} = 0.503$ and $\bar{C}_{sat} = 0.483$ mg m^{-3} respectively.

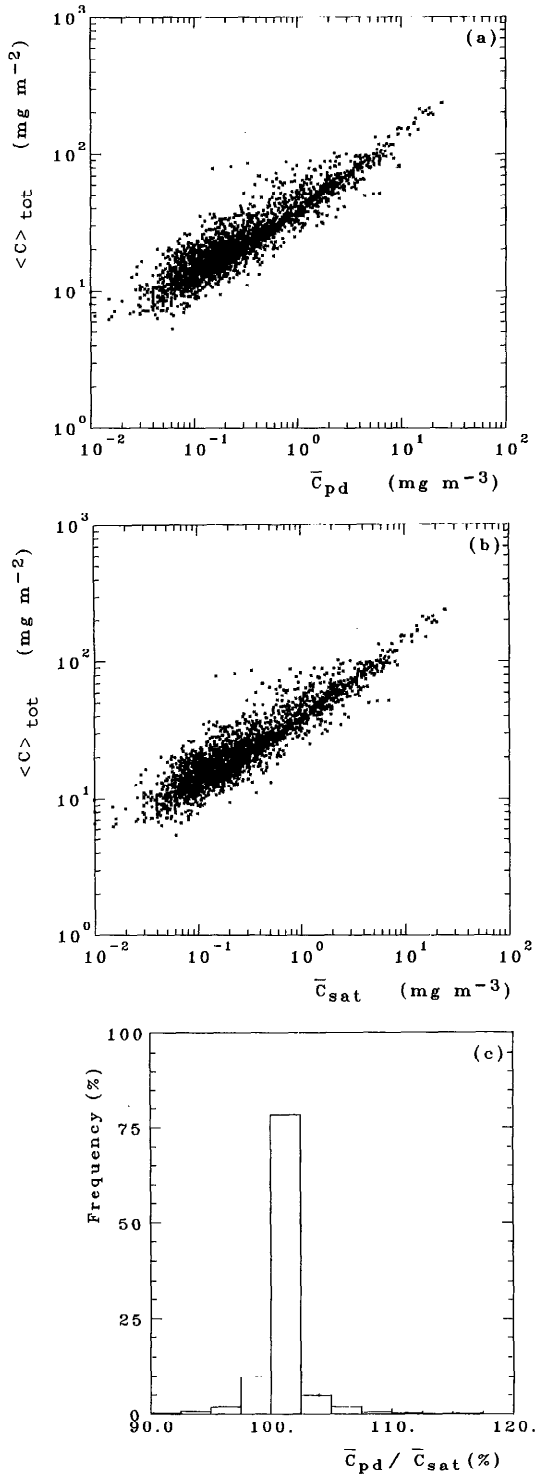

Fig. 3. a, b. Total pigment content $\langle C \rangle_{tot}$ within the euphotic layer vs. the mean pigment concentration $\bar{C}_{pd}$ within the surface layer and the weighted mean pigment concentration $\bar{C}_{sat}$ within the surface layer (3,806 stations; well-mixed waters stations excluded). c. Frequency distribution (expressed as percentage of the total number of stations) of the $\bar{C}_{pd}/\bar{C}_{sat}$ ratio.

20 equal layers ($\Delta\zeta = 0.1$) between the limits $\zeta = 0$ and $\zeta = 2$. Inside each layer the average normalized concentration was computed with the appropriate interpolations.

For stations where separate determinations of Chl *a* and Pheo *a* are available, it was also possible to compute the ratio

$$\rho = \text{Chl } a/(\text{Chl } a + \text{Pheo } a)$$

within each of the 20 layers and thereafter to derive a mean ρ profile pertinent to each trophic category.

Results

The results concerning the open ocean at low and moderate latitudes are examined first and those concerning the deep mixed layers (predominantly in the Antarctic zone) are presented next.

Total pigment content $\langle C \rangle_{tot}$ within the euphotic layer and mean pigment concentrations, $\bar{C}_{pd}$ and $\bar{C}_{sat}$, in the surface layer— The log-log plots of $\langle C \rangle_{tot}$ vs. $\bar{C}_{pd}$ (Fig. 3a) or vs. $\bar{C}_{sat}$ (Fig. 3b) both show a very regular trend, notwithstanding a more scattered distribution of the points in the low pigment concentration domain. This scattering reflects the impact of the variable deep chlorophyll maximum, which occurs almost systematically in oligotrophic situations. It is worth noting that the two distributions are very similar and the regression analyses over the whole concentration range (3,497 stations spanning over three orders of magnitude in terms of $\bar{C}_{pd}$ or $\bar{C}_{sat}$) lead to

$$\langle C \rangle_{tot} = 40.6\ \bar{C}_{pd}^{0.460} \qquad r^2 = 0.872 \quad (2a)$$

and

$$\langle C \rangle_{tot} = 40.6\ \bar{C}_{sat}^{0.459} \qquad r^2 = 0.869. \quad (3a)$$

A slight change in slope can be detected around 1.0 mg m^{-3}, so two separate regression analyses were performed, producing for the two domains the relationships given in Table 2 (Eq. 2b, c and 3b, c). The scattering of the points for $\bar{C}_{pd}$ (and $\bar{C}_{sat}$) $\leq$ 1 mg m^{-3}

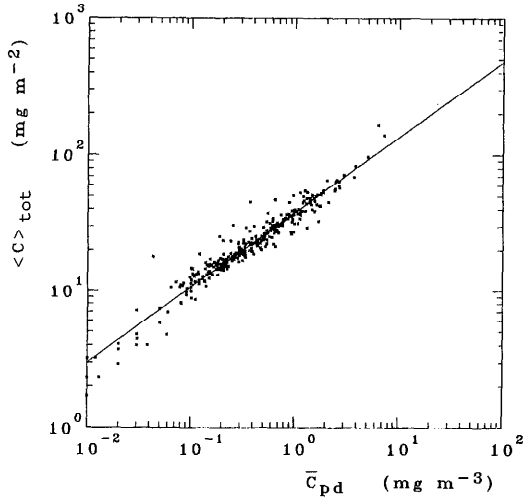

Fig. 4. Total pigment content $\langle C \rangle_{tot}$ within the euphotic layer vs. the mean pigment concentration $\bar{C}_{pd}$ within the surface layer for the 309 stations with well-mixed waters; the solid line corresponds to Eq. 4.

explains the lower correlation coefficient in this peculiar domain. The existence of deep biomasses in the low concentration domain accounts for the decrease of the exponent (from 0.507 and 0.505 in Eq. 2c and 3c to 0.425 and 0.423 in Eq. 2b and 3b).

Whatever the domain of concentration considered, the relationships involving $\bar{C}_{pd}$ and $\bar{C}_{sat}$ are practically confounded, so that arithmetic mean concentration or weighted mean concentration provide essentially the same result in terms of integrated chlorophyllous pigments (*see also* the histogram of the ratio $\bar{C}_{pd}/\bar{C}_{sat}$ in Fig. 3c).

Deep mixed-layer case—The Antarctic waters, selected as being located south of the Polar front, and the waters at or around Station P (about 53°N) during the winter season (14 profiles) are expected to be different from those previously studied. A careful (station by station) examination actually has demonstrated that these waters, even the most oligotrophic ones (including extremely clear waters observed in a polynia of the Weddell Sea by Gieskes et al. 1987), do not exhibit a distinct deep pigment maximum; only smooth features appear on several occasions.

The log-log plot of $\langle C \rangle_{tot}$ vs. $\bar{C}_{pd}$ is shown on Fig. 4 (the plot of $\langle C \rangle_{tot}$ vs. $\bar{C}_{sat}$, not shown here, is practically identical). The distribution of the points (309) is considerably less scattered than for the stratified situations: the quasi-absence of deep pigment maxima reduces the possible variability of the integrated pigment content with respect to the surface concentration. The corresponding relationships are

$$\langle C \rangle_{tot} = 38.0\ \bar{C}_{pd}^{0.551} \qquad r^2 = 0.933 \quad (4)$$

and

$$\langle C \rangle_{tot} = 37.9\ \bar{C}_{sat}^{0.548} \qquad r^2 = 0.930. \quad (5)$$

The rather homogeneous pigment concentration throughout the whole euphotic layer, including the surface layer, brings out higher correlations ($r^2 > 0.9$), as well as higher values of the exponents, than those obtained in the case of stratified waters.

Mean pigment profiles for each trophic category—Seven trophic categories were defined for the stratified waters and two for the well-mixed waters. Categorizing was made on the basis of the $\bar{C}_{pd}$ value because it is the remotely sensed observable quantity. However, by using the relationships established above between $\bar{C}_{pd}$ and $\langle C \rangle_{tot}$, the categories are as well defined with respect to integrated biomass. These categories (Table 3) represent waters ranging from very oligotrophic (with $\langle C \rangle_{tot} < 10.6$ mg m^{-2}) to very eutrophic ($\langle C \rangle_{tot} > 90.0$ mg m^{-2}) situations and include five intermediate situations for the stratified waters; only two trophic states (separated by $\bar{C}_{pd} = 0.45$ mg m^{-3}, or equivalently by $\langle C \rangle_{tot} = 27.1$ mg m^{-2}) have been distinguished in the case of cold mixed waters. The main results concerning each of these categories are displayed in Table 3. Mean concentration profiles of total pigment (Chl *a* + Pheo *a*) and of Chl *a* only are shown on Figs. 5 and 6 for stratified and unstratified waters. The total pigment profiles from Fig. 5 are pooled together in Fig. 7a (Fig. 7b is discussed later; *see Fig. 9 for profiles of the mean ratio* ρ).

In stable waters (Fig. 7a) most of the profiles exhibit a distinct deep maximum and, according to trophic state, a systematic evolution of this maximum is discernible which consists of:

- A diminution of its depth; distinctly encountered below the euphotic depth in oligotrophic situations (between 1.1 and

1.2 Z_e), the maximum is ascending in mesotrophic waters (profile e); insofar as it still exists, it would be close to or even at the surface in the most eutrophic situation, leading to a monotonic decreasing profile.

- In a parallel way, a remarkable diminution of its amplitude; the peak value is about 2.3 $\bar{C}_{Ze}$ (or five times the surface value) in the very oligotrophic situation, decreases for mesotrophic waters, and vanishes in the background for eutrophic waters.
- An increase of its width; relatively narrow for oligotrophic waters it tends to become broader when the integrated pigment content increases.
- There is a kind of hinge point at $Z = Z_e/2$, where C is close to $\bar{C}_{Ze}$, whatever the profile and the trophic state.

In well-mixed waters the deep maximum is virtually absent. The almost uniform profile (between 0 and Z_e) in Fig. 6 h is to be compared to that in Fig. 5 b relative to a similar trophic state, with $\langle C \rangle_{tot} = 14.6$ and 15.6 mg m^{-2}, respectively. In Fig. 6 h, $C/\bar{C}_{Ze}$ varies in the rather restricted range 0.9–1.1, instead of 0.6–1.8 as found in stratified waters. This also results in a near-surface concentration of $\bar{C}_{pd}$ twice that observed for stratified waters (0.2 instead of 0.1 mg m^{-3} on average, Table 3), whereas the 0–Z_e integrated pigments are nonetheless almost identical.

The difference between mixed and stratified waters weakens when situations from mesotrophic to eutrophic are considered. Comparable trophic states are illustrated by Fig. 6i and 5e (with $\langle C \rangle_{tot} = 39.5$ and 36.7 mg m^{-2}, respectively). Although the trends are opposite (regularly decreasing profile in Fig. 6i, increasing in Fig. 5e, with a maximum), the ranges of variation in $C/\bar{C}_{Ze}$ remain relatively narrow (0.9–1.1 in both cases). The average $\bar{C}_{pd}$ value is distinctly higher for well-mixed waters (1.2, instead of 0.8 mg m^{-3} in stratified waters).

The compatibility of these discrete data concerning the mean vertical distributions for selected situations and the continuous relationships previously derived between $\langle C \rangle_{tot}$ and $\bar{C}_{pd}$ (Eq. 2b, c and 4) must be verified. By integrating the profiles of Figs.

Table 3. Trophic categories (a–i) defined with respect to the mean pigment concentration within the surface layer C_{pd} and relevant parameters.

	Trophic category								
	a	b	c	d	e	f	g	h	i
$\bar{C}_{pd}$ range (mg m^{-3})	≤0.05*	0.05–0.15	0.15–0.30	0.30–0.45	0.45–1.50	1.50–5.00	≥5.00†	≤0.45‡	>0.45‡
No. of stations	117	1,089	894	379	557	392	69	173	136
Avg§ $\bar{C}_{pd}$ (mg m^{-3})	0.040	0.101	0.211	0.368	0.791	2.664	9.058	0.206	1.193
Avg§ $\langle C \rangle_{tot}$ (mg m^{-2})	9.99	14.58	19.70	25.33	36.73	65.15	124.15	15.63	39.54
Avg $\langle C \rangle_{1.5Z_e}$ (mg m^{-2})	20.57	28.84	36.68	42.33	59.15	98.07	195.27	27.43	69.45
Avg§ $\bar{C}_{Ze}$ (mg m^{-3})	0.105	0.197	0.336	0.525	0.994	2.622	8.455	0.230	1.215
$\langle C \rangle_{tot}$ computed‖ (mg m^{-2})	9.68	14.34	19.62	24.85	34.40	66.07	122.87	15.91	41.88
Avg§ Z_e (m)	99.4	79.4	63.3	52.9	41.2	26.5	16.9	79.4	40.4
Z_e computed¶ (m)	101.9	77.0	61.5	51.0	36.6	25.2	15.6	73.1	36.6
Deep pigment max, depth ζ	1.0–1.1	1.1–1.2	1.1–1.2	1.0–1.1	0.6–0.7	0.1–0.2	0.0–0.1	(1.0–1.1)	(0.0–0.1)
$C_{max}/\bar{C}_{Ze}$	2.3	1.8	1.6	1.2	1.0	(1.1)	(1.2)	(1.1)	(1.1)
$C_{max}/C_{(\zeta=0)}$	5.5	3.2	2.1	1.4	1.2	(1.0)	(1.0)	(1.2)	(1.0)
ρ (within the layer $\zeta = 0 \rightarrow 1$)	0.67	0.62	0.65	0.68	0.70	0.79	0.81	0.80	0.81

* Minimum value 0.01 mg m^{-3}.
† Maximum value 24.6 mg m^{-3}.
‡ Well-mixed waters only; minimum and maximum values 0.01 and 7.22 mg m^{-3}.
§ Average value of the parameter in question within each category.
‖ Computed with the average $\bar{C}_{pd}$ and Eq. 2b, c, and 4.
¶ Computed with the average $\langle C \rangle_{tot}$ and Eq. 1a and b.

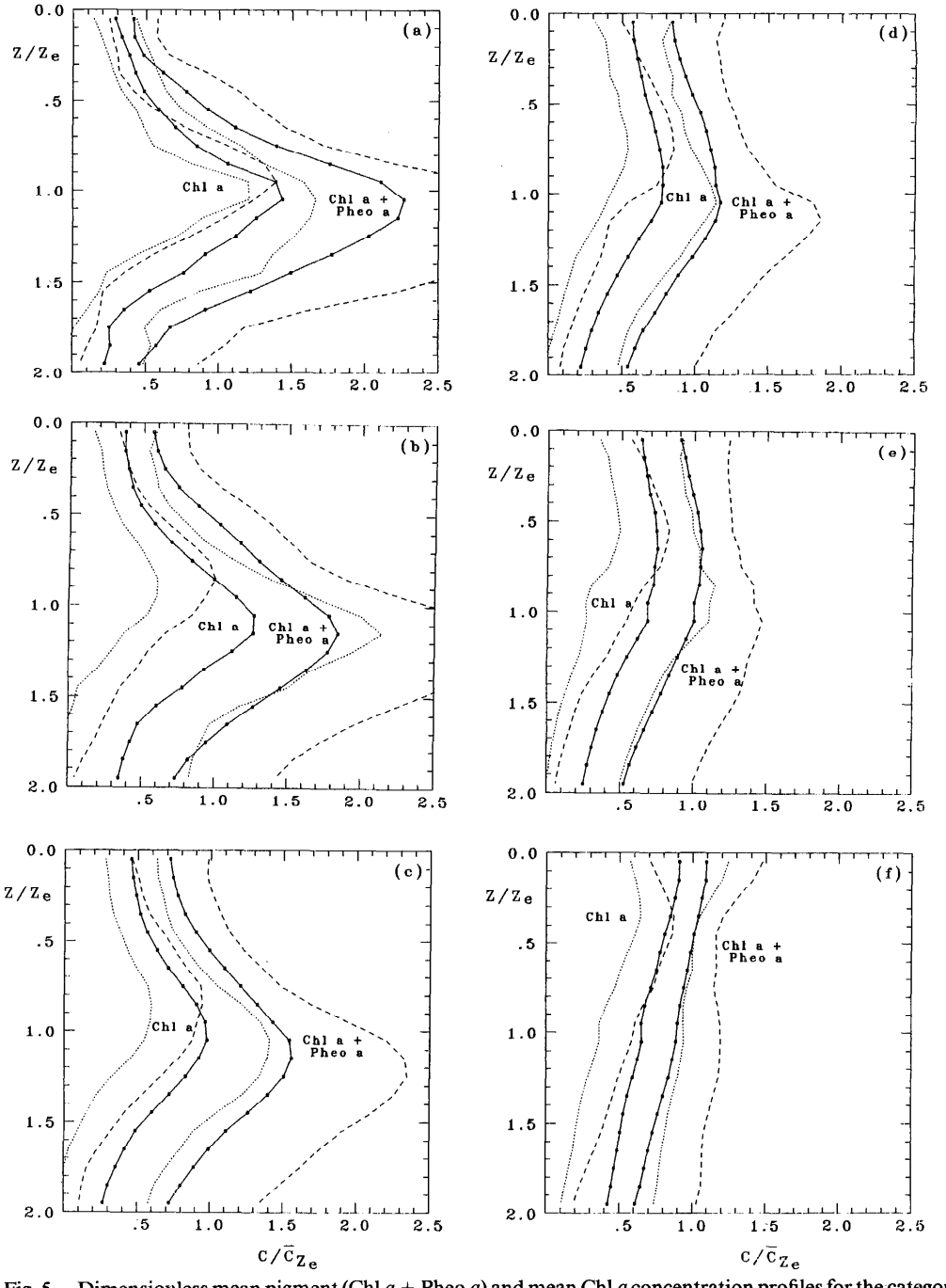

Fig. 5. Dimensionless mean pigment (Chl *a* + Pheo *a*) and mean Chl *a* concentration profiles for the categories defined by their $\bar{C}_{pd}$ values in Table 3 and labeled a–g. The dashed and dotted lines represent the limits $\pm \sigma$ where σ is the standard deviation for the two profiles.

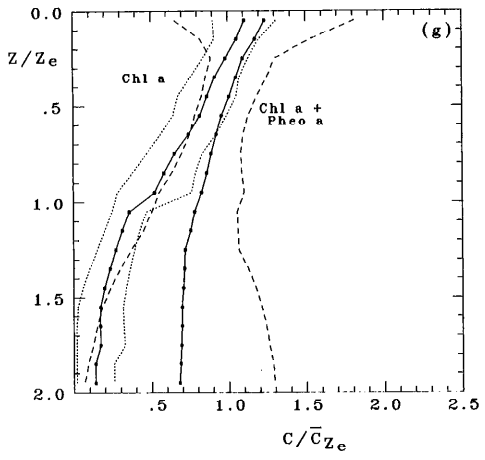

Fig. 5. Continued.

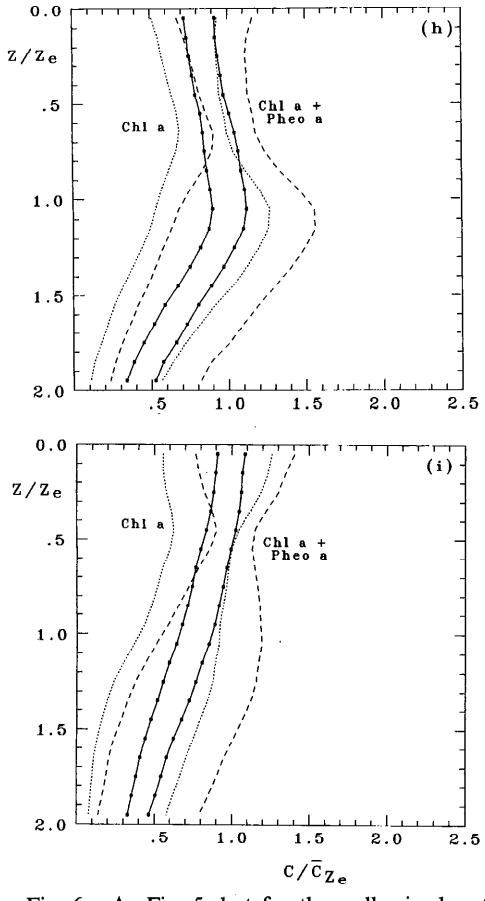

Fig. 6. As Fig. 5, but for the well-mixed waters categories (h and i in Table 3) defined by $\bar{C}_{pd} \leq 0.45$ or >0.45 mg m^{-3}. Dashed and dotted lines as for Fig. 5.

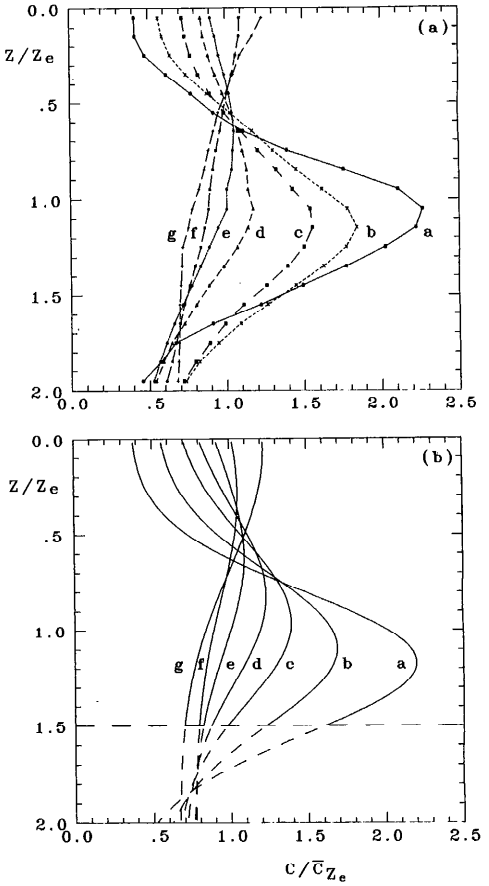

Fig. 7. Dimensionless mean pigment (Chl *a* + Pheo *a*) concentration profiles (a) redrawn from Fig. 5 and (b) computed according to Eq. 6 (*see text for the parameters*) with the mean $\bar{C}_{pd}$ values corresponding to each of the seven categories a–g (Table 3, line 5). Only the 0–1.5 Z_e depth interval was considered for the setting of the model.

5 and 6 over the appropriate layers (line $\bar{Z}_e$ in Table 3) and reintroducing the absolute values of $\bar{C}_{Ze}$ for each category (line 8 in Table 3), we obtain the corresponding $\langle C \rangle_{tot}$–$\bar{C}_{pd}$ values (Fig. 8). They are consistent with the continuous evolution depicted by Eq. 2b, c, and 4 represented as straight lines in the same figure. In addition, the pigment content integrated over an "extended" productive layer, i.e. from 0 to 1.5 Z_e, and denoted $\langle C \rangle_{1.5Ze}$, is also shown. It obviously amounts to about 1.5 $\langle C \rangle_{tot}$ in the homogeneous eutrophic situation or the oligotrophic well-mixed situation, whereas it reaches twice $\langle C \rangle_{tot}$ in the oligotrophic stratified

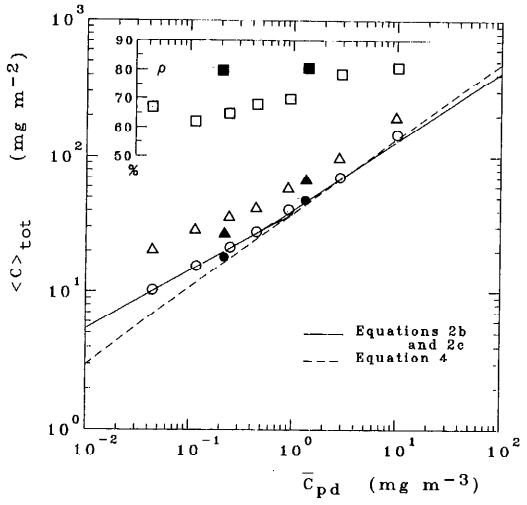

Fig. 8. Total pigment content $\langle C \rangle_{tot}$ within the euphotic layer vs. the mean pigment concentration $\bar{C}_{pd}$ within the surface layer. The solid and dashed lines correspond to Eq. 2b, c and Eq. 4 resulting from the regression analysis performed on the 3,497 stations of the stratified waters category and the 309 stations of the well-mixed waters category. Circles and triangles represent respectively the $\langle C \rangle_{tot}$ values and the pigment content integrated over the layer extended from 0 to 1.5 Z_e, both computed from the mean pigment concentration profiles. Inset represents the mean ratio ρ for the seven trophic (a–g) and two well-mixed waters categories (h–i). Open symbols designate the values pertaining to stratified waters and closed ones to well-mixed waters.

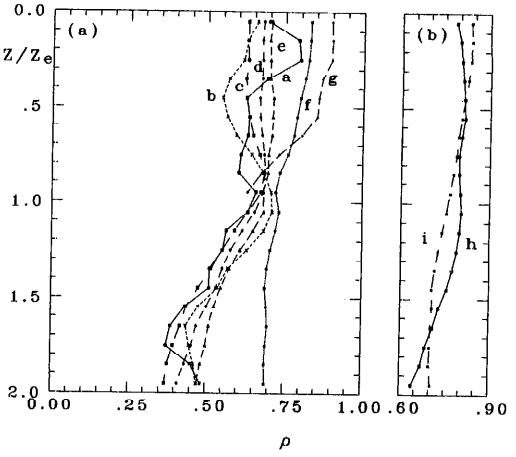

Fig. 9. Profiles of the mean ρ ratio, Chl *a*/(Chl *a* + Pheo *a*), profiles for the seven categories of stratified waters (a) and the two categories of well-mixed waters (b).

situations because of the presence of the deep maximum (*see also values in Table 3*).

Active chlorophyll and total chlorophyllous pigments—The mean Chl *a* profiles closely mimic those of total (Chl *a* + Pheo *a*) pigment in each of the trophic situations (Figs. 5, 6). Therefore the ρ ratio remains roughly constant, at least in the euphotic zone, as illustrated by Fig. 9. Noteworthy is that the value of this ratio decreases with a certain regularity from ~0.80 in eutrophic systems to 0.65 in oligotrophic waters (line 14 in Table 3 and also inset in Fig. 8). The same trend has been evidenced by Smith and Baker (1978, their figure 4). Beyond Z_e or 1.2 Z_e, this ratio significantly decreases for stratified waters whereas for cold waters (the profiles h and i in Fig. 9), ρ values are definitely higher than those observed in stable waters and seem to be practically constant between 0 and 2 Z_e, which supports the initial hypothesis of efficient vertical mixing.

We recognize that methodological problems (differences between spectrophotometric and fluorometric determination, interference of Chl *b* in the fluorometric determinations, among others) may generate some uncertainties in the ρ values presently used. A posteriori criticism of the data is not easy and the above conclusions must be regarded as tentative.

Discussion

Inferring the total pigment content from the upper layer concentration—Although making use of a much more restricted number of data, some previous studies have provided an insight into the $\langle C \rangle_{tot}$–$\bar{C}_{pd}$ relationships. The pioneer work by Lorenzen (1970) based on a statistical analysis of data from 91 stations resulted in an expression, $\langle C \rangle_{tot} = 33\ C_{surf}^{0.62}$, $r^2 = 0.817$, roughly compatible with those proposed here, except for the lowest concentration range. Later, Smith and Baker (1978) found a highly significant correlation ($r^2 = 0.95$, with data from 138 stations) over a wide range of concentration, expressed as

$$\overline{\mathrm{Chl}}_{Ze} = 0.955\ \overline{\mathrm{Chl}}_{pd}^{0.788}$$

where the subscripts have the same meanings as before, but $\overline{\mathrm{Chl}}$ replaces $\bar{C}$, since this

statistical analysis dealt with Chl *a* only. When combined with the empirical equation 3 of Morel (1988), Eq. 2a (also established for the entire concentration range and for stable waters), leads to

$$\bar{C}_{Ze} = 1.12\ \bar{C}_{pd}^{0.803}.$$

The consistency between these two nonlinear expressions is satisfying, especially when we consider that the ratio $\overline{Chl}/\bar{C}$ is slightly varying. They simply express that the mean pigment concentration within the euphotic layer becomes either higher or lower than the concentration in the upper layer depending on whether the latter is below or above 1 mg m^{-3} (*see also Table 3*). Using a set of data from 128 stations (all included in the present study), Bricaud (1989) obtained relationships between $\langle C\rangle_{tot}$, $\bar{C}_{pd}$, and $\bar{C}_{sat}$ that are consistent with those presented above.

We therefore believe that the mean or the total pigment content within the euphotic layer (or even within a layer 1.5 times thicker) can be inferred solely from knowledge of the mean pigment concentration within the remotely detectable upper layer, $\bar{C}_{sat}$ or $\bar{C}_{pd}$ (which are practically identical: within ±2.5%, *see Fig. 3c*). Instead of using a single relationship (Eq. 2a), it is certainly more reliable to distinguish between two trophic situations (divided by $\bar{C}_{pd}$ = 0.5 mg m^{-3}) and to use the two distinct equations (Eq. 2b and c) to derive $\langle C\rangle_{tot}$. In spite of lower r^2 values, these equations are more consistent with the general evolution of the vertical profiles and its consequences on the $\langle C\rangle_{tot}$ variations, as is substantiated by Fig. 8.

Unusual events in the vertical pigment distribution very likely occur and obviously cannot be accounted for by relationships based on statistical averages. The significance of the correlations as obtained is, however, very encouraging and ensures a good probability of properly estimating $\langle C\rangle_{tot}$ in most oceanic situations. It is acknowledged that winter situations with deep convection and extended mixed layers are not sufficiently documented and deserve further investigation. There is every evidence that quasi-uniform vertical profiles prevail for such situations and it is believed that Eq. 4 can be used as a first approach when dealing with such cold, destabilized waters.

Inferring the biomass profile when it is not uniform (stratified waters)—For these waters it is possible to adopt a typical profile, with the usual reservation attached to the use of statistical averages. A simple way is just to categorize the water according to its trophic state in terms of $\bar{C}_{pd}$ or $\langle C\rangle_{tot}$ and to select one of the profiles in Fig. 5 or, if needed, to interpolate between these profiles.

It can be imagined that the shape of these profiles is continuously modified as a function of $\bar{C}_{pd}$ or $\langle C\rangle_{tot}$, and upon such a hypothesis, it is tempting to model this change by means of an adequate parameterization. If we restrict the model to the 0–1.5 Z_e depth interval, the generalized Gaussian profile (Lewis et al. 1983) can be adopted to reproduce the actual profiles. A numerical analysis of the $C(\zeta)/\bar{C}_{Ze}$ profiles in Fig. 7a as a function of $\bar{C}_{pd}$ (denoted c in equations below) leads to a possible parameterization:

$$C(\zeta)/\bar{C}_{Ze} = C_b + C_{max}\exp\{-[(\zeta - \zeta_{max})/\Delta\zeta]^2\} \quad (6)$$

with

$$C_b = 0.768 + 0.087 \log c - 0.179(\log c)^2 - 0.025(\log c)^3,$$
$$C_{max} = 0.299 - 0.289 \log c + 0.579(\log c)^2,$$
$$\zeta_{max} = 0.600 - 0.640 \log c + 0.021(\log c)^2 + 0.115(\log c)^3,$$

and

$$\Delta\zeta = 0.710 + 0.159 \log c + 0.021(\log c)^2$$

where C_b is a background over which is superimposed a Gaussian curve with a maximum value given by C_{max}, occurring at ζ_{max}, and having a thickness controlled by $\Delta\zeta$; all these profile characteristic parameters are made to vary with c. The modeled profiles, computed with the mean $\bar{C}_{pd}$ values corresponding to each category defined in Table 3 (line 4), are shown for comparison on Fig. 7b. They reproduce the actual profiles fairly well. It must be emphasized that use of the above parameterization must be restricted to the range of $\bar{C}_{pd}$ values extending from

about 0.02 to 10 mg m^{-3}, namely the range envisaged when fitting the analytical equations to the actual profiles.

For practical use, once the above equations have been operated to produce the profile, the dimensionless depth ζ must then be restored to a geometrical depth by Eq. 1a (or 1b) used in conjunction with the $\langle C \rangle_{tot}$ value also derived from $\bar{C}_{pd}$ (equations in Table 2).

The profile of the active biomass, expressed in terms of Chl *a* concentration, can be derived straightforwardly from the previous profile of Chl *a* + Pheo *a*, as the ratio ρ appears to be a rather monotonic function of $\langle C \rangle_{tot}$ (Table 3 and Fig. 8) and also to be constant with respect to depth, at least in first approximation.

Use of the remotely sensed pigment concentration to infer the potential carbon fixation by algae—A simple way, already explored (Smith et al. 1982; *see also* Bricaud 1989 and references therein), consists of assuming a constant proportionality between the carbon fixation per unit of Chl *a* present within the euphotic zone and $\overline{PAR}(0^+)$, the photosynthetically available radiation impinging at the surface according to

$$\overline{PSR} = \overline{PAR}(0^+) \langle Chl \rangle_{tot} \psi^* \quad (7)$$

where $\overline{PSR}$ is the photosynthetically stored energy within the euphotic zone and ψ^* is the cross-section for photosynthesis per unit of areal chlorophyll. The overbars on PSR and PAR denote daily integrated quantities, both expressed as J m^{-2}. The fixation of 1 mg of carbon corresponds to a storage of 39 J, and $\overline{PSR}$ is readily converted into P (the amount of carbon incorporated into the algal biomass per day).

With $\langle C \rangle_{tot}$ expressed as a function of the remotely sensed pigment concentration and recalling that active chlorophyll is only a fraction of ρ of this chlorophyllous pigment content, Eq. 7 can be rewritten.

$$P = (1/39)\, \overline{PAR}(O^+)\, \rho\, F(\bar{C}_{pd})^E\, \psi^* \quad (8)$$

where F and E are the factors and exponents appearing in Eq. 2b and c. This equation can be used for the seven trophic categories defined in Table 3 with, as example, $\overline{PAR}(0^+)$ = 11.47 MJ (the value computed for a clear sky at the Tropic of Cancer and for the vernal equinox; *see* Morel 1989) and with ψ^* = 0.07 m^2 (g Chl)$^{-1}$, a mean value previously derived from field experiments (Morel 1978). The results of such simplified computations are given in Table 4 (line 1).

Given that the knowledge of $\bar{C}_{pd}$ allows not only $\langle C \rangle_{tot}$ but also the vertical biomass profile to be determined (or modeled according to Eq. 6), an improved method consists of operating a spectral light-production model in conjunction with the actual profile. This procedure is applied to the seven profiles for stratified waters. The photosynthetic radiant energy is propagated by using the profile of Chl *a* + Pheo *a* concentration according to a scheme previously described (Morel 1988), whereas carbon fixation is computed by using the active pigment profile (the Chl *a* concentration at each level).

The results obtained by using a model presented elsewhere (Morel 1989) are given in Table 4 (lines 2, 3) in terms of integrated production for the euphotic layer (and also for an extended productive layer comprised between 0 and 1.5 Z_e). The model is run with the standard set of physiological parameters (*see* Morel 1989), a uniform temperature of 20°C, and for the Tropic of Cancer on 21 March, as before. Integrated productions are slightly lower than those obtained when applying the global Eq. 8. This lowering originates from the fact that ψ^* is sensitive to the radiative energy level and is depressed when this level increases. For the day and latitudes adopted, the $\overline{PAR}(0^+)$ value is rather high and the light-photosynthesis model, in effect, produces variable ψ^* values (Table 4, line 4) that are slightly below the constant mean value introduced in Eq. 8.

The production profiles corresponding to the seven categories are plotted in absolute units (logarithmic scale) as a function of ζ in Fig. 10a. The shape of these profiles is more clearly revealed on Fig. 10b where local production is normalized with respect to the mean value computed within the interval 0 to Z_e and plotted on a linear scale. The maximum of production occurs at $\zeta \simeq 0.8$ in very oligotrophic waters, i.e. above the deep Chl maximum (at $\zeta > 1.1$) and migrates toward the surface, reaching ζ = 0.2 or 0.1 in the case of eutrophic waters;

Table 4. Daily (21 March, Tropic of Cancer) production P, as mg C m^{-2} d^{-1}, within the euphotic layer (0–Z_e) or within an extended layer (0–1.5 Z_e) and Chl-specific cross-section for photosynthesis, ψ^*, as m^2 (g Chl)$^{-1}$, computed for the seven categories by operating either Eq. 8 or a light-production model. The mean ratio ρ for each category is also indicated (bottom).

	Trophic category						
	a	b	c	d	e	f	g
$P(0,Z_e)$†	0.133	0.183	0.262	0.348	0.496	1.074	2.049
$P(0,Z_e)$‡	0.110	0.161	0.236	0.325	0.482	0.916	1.784
$P(0,1.5Z_e)$‡	0.132	0.193	0.269	0.359	0.523	0.974	1.843
$\psi^*(0,Z_e)$‡	0.0567	0.0572	0.0585	0.0595	0.0593	0.0583	0.0561
$P(0,Z_e)$§	0.123	0.170	0.245	0.331	0.481	0.891	1.616
$P(0,1.5Z_e)$§	0.138	0.189	0.273	0.366	0.527	0.961	1.724
$\psi^*(0,Z_e)$§	0.0609	0.0610	0.0608	0.0603	0.0594	0.0571	0.0538
ρ‖	0.67	0.62	0.65	0.68	0.70	0.79	0.81

† Production computed with Eq. 8 and $\psi^* = 7\times10^{-3}$ m^2 (g Chl)$^{-1}$.
‡ P computed with the light-production model in conjunction with the mean pigment profiles of Fig. 7a and the ρ values given in the last line; P is computed for the layer $(0,Z_e)$ or the layer $(0,1.5Z_e)$, whereas ψ^* is given only for the $(0,Z_e)$ layer.
§ As above, except that uniform pigment profiles with the same integrated $(0,Z_e)$ pigment content, replace the nonuniform profiles of Fig. 7a.
‖ Mean ρ value for each of the seven categories, with ρ = Chl *a*/(Chl *a* + Pheo *a*).

it does not reach the very surface due to the inhibition effect, which is accounted for in the model. Interestingly, the relative importance of carbon fixation occurring at deep levels, beyond the depth of the euphotic zone, is far from negligible in the oligotrophic situation (+20% with respect to the production realized between 0 and Z_e; *see Table 4 and Fig. 10b*). As expected from the profile evolution with the trophic state, the contribution of this deep production regularly decreases and practically vanishes (+3%) in the most eutrophic waters

It is worthwhile to quantify the impact of the nonuniformity in the vertical biomass profile on production. This can be simply effected by running the model again and holding all the parameters unchanged, except that uniform profiles with the mean $\bar{C}_{Ze}$ value replace the previous structured profiles, so that $\langle C\rangle_{tot}$ remains constant (this $\bar{C}_{Ze}$ value is also extended down to 1.5 Z_e). The corresponding profiles, normalized as before, are shown in Fig. 10c and the integrated production values are given in Table 4 (lines 5, 6). Obviously no significant change occurs for eutrophic waters, which were almost perfectly homogeneous. As can be anticipated, the larger departure actually occurs for oligotrophic situations. It remains, however, surprisingly weak with only a 12% (situation a) or 6% (situation b) increase in production when the same amount of chlorophyll is uniformly dispersed within the entire euphotic layer instead of being concentrated at the bottom of this layer.

It must be emphasized that $\bar{C}_{Ze}$ is largely higher than $\bar{C}_{pd}$ in most of the oceanic waters and especially in oligotrophic zones (*see Table 3*). Therefore, production would be seriously underestimated if the $\bar{C}_{pd}$ value, as remotely sensed, was directly (and erroneously) used and extended down to Z_e. For instance, the underestimation which would result from using $\bar{C}_{pd}$ in place of $\bar{C}_{Ze}$ when computing carbon fixation amounts to 45% in situation a.

This analysis demonstrates that for the purpose of estimating production, the above profile parameterization (Eq. 6) is certainly sufficient, even if imperfect. A more important consequence emerges; it is widely admitted that the shape of the biomass profile is of crucial importance in governing production capabilities. This opinion, sound in principle and realistic when facing individual situations with chaotic profiles, must be revised within a global and geochemical perspective which necessarily copes with the obligation of using statistical averages. The shapes of the mean profiles, as they result from the present statistical analysis, do not appear as having a noticeable influence on the computed production, under the proviso that computation is performed with a representative mean (or total) pigment val-

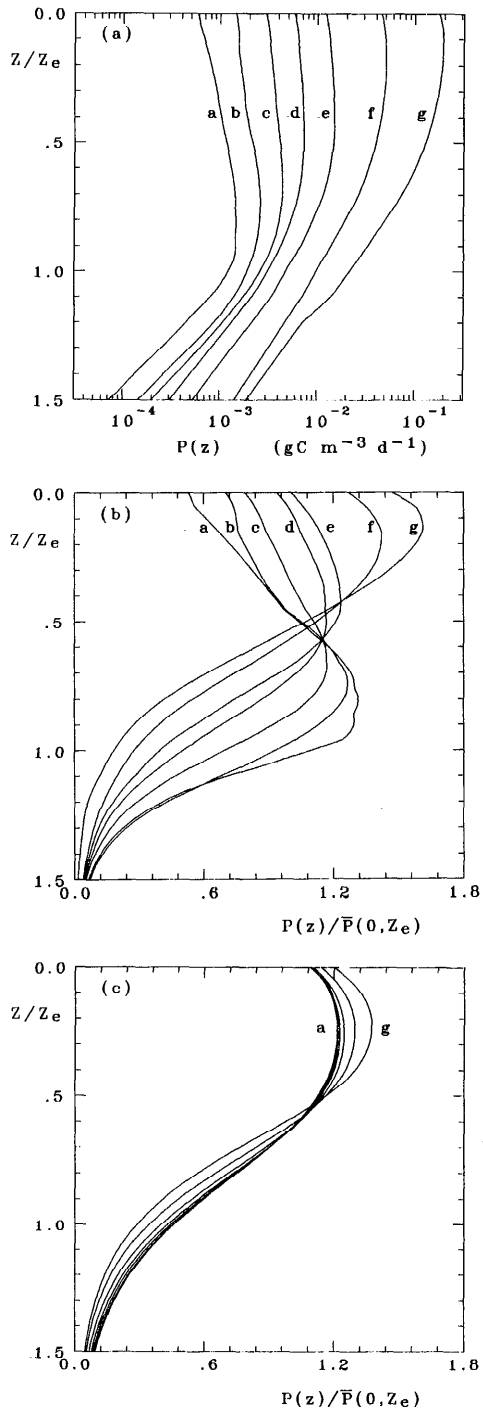

Fig. 10. Daily production profiles as a function of Z/Z_e, computed by operating a spectral light-production model (Morel 1989) in conjunction with the biomass profiles of the seven categories a–g (*see also Table 4*) (a) in absolute units (g C m^{-3}) and (b) in dimensionless units: $P(z)$ is normalized with respect to its mean value within the interval $z = 0$ to $z = Z_e$. Production computed for uniform profiles with the mean concentration $\bar{C}_{Ze}$ extended down to 1.5 Z_e (c), also in dimensionless units; all computations are carried out for the Tropic of Cancer and 21 March.

ue for the euphotic zone and definitely not with the remotely sensed upper surface value (generally much lower than $\bar{C}_{Ze}$). In addition, the above estimates of production occurring within the deep maximum (or below Z_e) must be seen as upper limits, to the extent that a constant temperature is assumed in the computation, whereas in the natural environment, lower temperatures and depressed productions are expected at these deep levels.

Recent studies have addressed the nature of the nonuniform vertical structure of pigments in relation to estimates of production. In the study by Sathyendranath et al. (1989), an approach was used that was very different from the one presented here. They made use of a generalized Gaussian profile of pigments in order to perform a sensitivity analysis for the model of production. With this objective, various nonuniform profiles were generated by varying one-by-one and independently each of the four parameters (which govern the profile) over a range of "plausible values" and primary productions were then computed. For such a numerical exercise, the range is slightly exaggerated to more clearly obviate trends in the resulting production. By comparing these productions with those computed for uniform profiles, the impact of nonuniformity is expressed in terms of "relative error."

The work presented here is aimed at delimiting the plausible values before going further. The use of dimensionless depths has been revealed to be fruitful, inasmuch as a natural order has emerged that was not apparent when the profiles were scaled according to geometrical depths. The consequence of this ordering is that the four parameters of the profiles (Eq. 6) are interlinked because they are all related to the trophic state, depicted by $\langle C \rangle_{tot}$ or even by $\bar{C}_{pd}$. These relationships introduce realistic constraints when computing carbon fixa-

tion; as a result of these constraints, the possible excursion of the "errors" is here more restricted than in the numerical experiment of Sathyendranath et al. (1989).

For instance, the errors they computed when the depth of the deep maximum is varied are in the same direction as those shown here when this depth is assigned to remain close to Z_e (as statistically observed), but they are not of the same magnitude. Their figures 8c (uniform profile constructed with the mean chlorophyll concentration, i.e. with $\bar{C}_{Ze}$ in our notation) and 10c (constructed with the satellite-weighted chlorophyll, i.e. with $\bar{C}_{pd}$) show more significant errors than the differences (between uniform and nonuniform profiles) shown in Table 4 and mainly results from the peak value they selected, which is as high as 15 times the background value, instead of 5.5 (at most) in the oligotrophic waters of situation a (Table 3).

The important and practical consequence of the present statistical analysis on the production computation is that the shape of the profile is, on average, of relatively weak influence provided that $\langle C \rangle_{\text{tot}}$ is correctly estimated (recall that the $\langle C \rangle_{\text{tot}}$ value accounts for the existence of an average peak). A more crucial parameter is the ρ ratio which responds almost linearly to the production estimates. Also due attention must be paid to deep production (below Z_e), which is certainly not negligible in many oligotrophic or even mesotrophic waters widely represented in the world ocean.

Conclusion

It is unreasonable and probably superfluous to envisage the use of a light-production model on a pixel-by-pixel basis when interpreting satellite imagery. The use of an expression like Eq. 8 is a safer and much faster way, provided that the use of a single "mean" ψ^* value is abandoned and that more adapted, i.e. seasonally and zonally variable, ψ^* values are introduced. In other words, a climatological field of the ψ^* parameter must be produced by operating the light-production model for various dates and latitudes and also for the various trophic conditions characterized in particular by their biomass profiles. The limitations of such a model, as discussed elsewhere (Morel 1989), essentially result from the uncertainties which presently exist about the physiological parameters to be entered into the computations. We therefore recommend that field efforts be focused on the acquisition of a better knowledge of these parameters and their possible variations. Gathering more information about the vertical biomass profiles, including the typical ρ values is also desirable (for ρ, historical data may have been biased because of methodological deficiencies). An increased data bank could reinforce confidence in the statistical relationships proposed here and will improve the use of remotely sensed data to estimate the CO_2 flux entering the marine phytosphere.

References

ALVAREZ-BORREGO, S., AND G. GAXIOLA-CASTRO. 1988. Photosynthetic parameters of northern Gulf of California phytoplankton. Continental Shelf Res. **8:** 34–47.

ANDERSON, G., R. LAM, B. BOOTH, AND J. GLASS. 1977. A description and numerical analysis of the factors affecting the processes of production in the Gulf of Alaska. Univ. Washington, Dep. Oceanogr. Spec. Rep. 76.

ANTIPROD 1. 1978. Groupe Mediprod. Résultats des Campagnes à la Mer. Publ. CNEXO No. 16. 151 p.

ANTIPROD 2. 1982. Campagne Océanographique MD 21. Com. Natl. Fr. Rech. Antarct. No. 53. 141 p.

APSARA 2—ANTIPROD 3. 1987. Les rapports des Campagnes à la Mer. Publ. Mission Rech. T.A.A.F. No. 84-01. 345 p.

BERGER, W. H., K. FISHER, C. LAI, AND G. WU. 1987. Ocean productivity and organic carbon flux. Part 1. Overview and maps of primary production and export production. Scripps Inst. Oceanogr. SIO Ref. 87-30. 67 p.

BRICAUD, A. 1989. Propriétés optiques du phytoplancton: Étude théorique et expérimentale. Application à l'interprétation de la couleur de la mer. D.S., Univ. Pierre et Marie Curie, Paris 6. 163 p.

BROWN, P. C., AND J. L. HENRY. 1985. Phytoplankton production, chlorophyll *a* and light penetration in the southern Benguela Upwelling region during the period between 1977 and 1980, p. 211–218. *In* South African ocean color and upwelling experiment. Sea Fish. Res. Inst. Cape Town.

CALYPSO. 1969. Résultats des observations effectuées en Mer Tyrrhénienne à bord du navire Océanographique "Calypso" en juillet 1964. Cah. Oceanogr. 21(suppl. 2), p. 193–202.

CUEA JOINT 1. 1975. Data Rep. 14. 165 p.

CUEA-JOINT 2. 1977. Data Rep. 49. 476 p.

CULLEN, J. J. 1982. The deep chlorophyll maximum: Comparing vertical profiles of chlorophyll *a*. Can. J. Fish. Aquat. Sci. **39:** 791–803.

DANDONNEAU, Y. 1979. Concentrations en chlorophylle dans le Pacifique tropical sud-ouest: Comparaison avec d'autres aires océaniques tropicales. Oceanol. Acta **2:** 133–142.

ELBRÄCHTER, M., AND OTHERS. 1987. Phytoplankton and heterotrophic microorganisms in the water column. Polar Res. **39:** 190–196.

GIESKES, W. W. C., C. VETH, A WOEHRMANN, AND M. GRAEFE. 1987. Secchi disc visibility world record shattered. Eos **68:** 123.

GLOVER, D. M., AND P. G. BREWER. 1988. Estimate of wintertime mixed layer nutrient concentrations in the North Atlantic. Deep-Sea Res. **35:** 1525–1546.

GOFFART, A., AND J. H. HECQ. 1988. Distribution of phytoplanktonic parameters in the Indian sector of the Southern Ocean during INDIGO 3 cruise, p. 148–166. *In* Proc. Belg. Natl. Colloq. Antarc. Res. P.M. Serv.-Sci. Policy Office.

GORDON, H. R., AND W. R. MCCLUNEY. 1975. Estimation of the depth of sunlight penetration in the sea for remote sensing. Appl. Opt. **14:** 413–416.

HECQ, J. H., AND OTHERS. 1986. Some aspects of the Liguro-Provençal frontal ecohydrodynamics, p. 257–271. *In* Marine interface ecohydrodynamic. Elsevier Oceanogr. Ser. V. 42.

HERBLAND, A., AND B. VOITURIEZ. 1979. Hydrological structure analysis for estimating the primary production in the tropical Atlantic Ocean. J. Mar. Res. **37:** 87–101.

IGBP. 1988. The International Geosphere-Biosphere Programme: A study of global change. IGBP Rep. 4. 200 p.

INNAMORATI, M., AND OTHERS. 1989*a*. Phytoplankton populations and hydrobiological conditions of Tuscan Archipelago [in Italian]. Campagna Elba 1 and 2. Rep. Proc. Mare 6. Univ. Florence. 70 p.

———, G. MORI, G. CATALANO, AND F. BENEDETTI. 1989*b*. Distribution of phytoplankton biomass with reference to ambient factors in the Ross Sea (Terranova Bay): Antartide 2 [in Italian]. 1st Ital. Occanogr. Exped. to the Ross Sea. Rep. Proc. Mare 4. Univ. Florence. 58 p.

INDIGO 1. 1988. Les rapports des Campagnes à la Mer. Publ. Mission Rech. T.A.A.F. No. 85-06. 267 p.

JAMART, B. M., D. F. WINTER, K. BANSE, G. C. ANDERSON, AND R. K. LAM. 1977. A theoretical study of phytoplankton growth and nutrient distribution in the Pacific Ocean off the northwestern U.S. coast. Deep-Sea Res. **24:** 753–773.

JGOFS. 1988. Report of the first session of the SCOR committee for JGOFS. Sci. Comm. Ocean. Res. 50 p.

LAWS, E. A., G. R. DITULLIO, AND D. G. REDALJE. 1987. High phytoplankton growth and production rates in the North Pacific subtropical gyre. Limnol. Oceanogr. **32:** 905–918.

LEVITUS, S. 1982. Climatological atlas of the world ocean. NOAA Prof. Pap. 13. NOAA, Rockville, 173 p.

LEWIS, M. R., J. J. CULLEN, AND T. PLATT. 1983. Phytoplankton and thermal structure in the upper ocean: Consequences of nonuniformity in chlorophyll profile. J. Geophys. Res. **88:** 2565–2570.

LORENZEN, C. J. 1970. Surface chlorophyll as an index of the depth, chlorophyll content, and primary productivity of the euphotic layer. Limnol. Oceanogr. **15:** 479–480.

MARTIN, J. H., G. A. KNAUER, D. M. KARL, AND W. W. BROENKOW. 1987. VERTEX: Carbon cycling in the northeast Pacific. Deep-Sea Res. **34:** 267.

MEDIPROD 1. 1971. Résultats de la Campagne Mediprod 1, p. 93–144. *In* Cah. Oceanogr. No. 23, Spec. Issue.

MOREL, A. 1978. Available, usable, and stored radiant energy in relation to marine photosynthesis. Deep-Sea Res. **25:** 673–688.

———. 1988. Optical modelling of the upper ocean in relation to its biogenous matter content (Case 1 waters). J. Geophys. Res. **93:** 10,749–10,768.

———. 1989. Light and marine photosynthesis: A model with geochemical and climatological implications. Prog. Oceanogr. In press.

———, AND L. PRIEUR. 1977. Analysis of variations in ocean color. Limnol. Oceanogr. **22:** 709–722.

PACIPROD. 1989. Résultats des campagnes à la mer. Publ. Ifremer 7. 183 p.

PLATT, T., AND S. SATHYENDRANATH. 1988. Oceanic primary production: Estimation by remote sensing at local and regional scales. Science **241:** 1613–1620.

———, ———, C. M. CAVERHILL, AND M. R. LEWIS. 1988. Ocean primary production and available light: Further algorithms for remote sensing. Deep-Sea Res. **35:** 855–879.

SATHYENDRANATH, S., T. PLATT, C. M. CAVERHILL, R. E. WARNOCK, AND M. R. LEWIS. 1989. Remote sensing of oceanic primary production: Computations using a spectral model. Deep-Sea Res. **36:** 431–453.

SCOR—WORKING GROUP 15. 1973. Data report SCOR *Discoverer* expedition. Scripps Inst. Oceanogr. SIO Ref. 73-16. V. 2.

SEAWIFS. 1987. Report of the joint EOSAT/NASA SeaWIFS working group. NASA-EOSC. 91 p.

SMITH, R. C., AND K. S. BAKER. 1978. The bio-optical state of ocean waters and remote sensing. Limnol. Oceanogr. **23:** 247–259.

———, R. W. EPPLEY, AND K. S. BAKER. 1982. Correlation of primary production as measured aboard ship in southern California coastal waters and as estimated from satellite chlorophyll images. Mar. Biol. **66:** 281–288.